


# Influence of Hot Deformation on the Precipitation Hardening of High-Strength Aluminum AA7075 during Thermo-Mechanical Processing

Emad Scharifi \* , Daria Shoshmina, Stefan Biegler, Ursula Weidig and Kurt Steinhoff

Metal Forming Technology, University of Kassel, Kurt-Wolters-Straße 3, 34125 Kassel, Germany; shoshmina@googlemail.com (D.S.); StefanBiegler@gmx.de (S.B.); ursula.weidig@uni-kassel.de (U.W.); steinhoff@uni-kassel.de (K.S.)

\* Correspondence: emad.scharifi@uni-kassel.de; Tel.: +49-56-1804-1973

**Abstract:** The aim of this work was to investigate the effect of hot deformation on the aging behavior of precipitation-hardenable aluminum alloy AA7075 within a novel thermo-mechanical forming process, in order to gain insight into its precipitation kinetics. For this purpose, the material was formed at 420 °C after undergoing solution treatment to different strain levels ranging from 2% to 10% to obtain different dislocation densities. After undergoing hot deformation, aging at 120 °C with different parameters was carried out to improve the material hardness. The resulting material properties and microstructure evolution were characterized afterward using hardness measurements and a transmission electron microscope (TEM). TEM investigations revealed the formation of very fine particles for the material formed at 2%, as well as at 10%, of formed material, which act as effective barriers to dislocation motion. It was found that the response of artificial aging on the deformation degree in hot forming was less than expected due to the thermally activated mechanisms, leading to a decrease in dislocation density. Therefore, a dramatic increase in material hardness with the increase in hot deformation was not observed.

**Keywords:** thermo-mechanical processing; precipitation-dislocation hardening; recrystallization; high strength aluminum alloys; hot deformation



**Citation:** Scharifi, E.; Shoshmina, D.; Biegler, S.; Weidig, U.; Steinhoff, K. Influence of Hot Deformation on the Precipitation Hardening of High-Strength Aluminum AA7075 during Thermo-Mechanical Processing. *Metals* **2021**, *11*, 681. <https://doi.org/10.3390/met11050681>

Academic Editor: Marcello Cabibbo

Received: 24 March 2021

Accepted: 18 April 2021

Published: 21 April 2021

**Publisher's Note:** MDPI stays neutral with regard to jurisdictional claims in published maps and institutional affiliations.



**Copyright:** © 2021 by the authors. Licensee MDPI, Basel, Switzerland. This article is an open access article distributed under the terms and conditions of the Creative Commons Attribution (CC BY) license (<https://creativecommons.org/licenses/by/4.0/>).

## 1. Introduction

Despite their limited cold formability, precipitation-hardenable aluminum alloys represent a high potential for application to modern automotive and aerospace industries, due to their excellent strength-to-weight ratios and their fatigue and cryogenic toughness properties [1,2]. For this reason, different forming processes at room and elevated temperatures have been proposed to overcome this limitation of high-strength aluminum alloys [3–6]. One of the promising techniques that allows the realization of complex-shaped structures was first proposed by Lin et al. [7]. This forming process combines hot forming and quenching of the heated sheet material after solution heat treatment using cooled forming tools. Accordingly, by using this technique, due to the high-temperature forming, a better formability and extremely low springback were obtained compared to that formed at room temperature [8–11]. In addition, the integrated cooling during the forming operation enables high cooling rates and the creation of a supersaturated solid solution (SSSS) after solutionizing, which is needed to generate precipitate nucleation during aging treatment in the case of precipitation-hardenable aluminum alloys [12–15].

Wang et al., for example, investigated the influence of different forming temperatures, ranging from 350 °C to 493 °C, on the forming behavior of AA2024 [16]. The results of their study revealed an intense increase in total elongation of the material up to 450 °C due to the thermally activated softening mechanisms. A similar trend was observed for AA7075 tested at high temperatures ranging from 200 °C to 400 °C [17]. The investigated microstructure

in this study showed a high fraction of low-angle grain boundaries at 200 °C compared to those at 400 °C. From the microstructural analysis, it was concluded that dynamic recovery is the dominant softening mechanism for AA7075 formed at 200 °C, whereas at the higher deformation temperature of 400 °C, the occurrence of dynamic recrystallization causes the intense softening of the material. The recrystallized microstructure was detected using the electron backscatter diffraction (EBSD) technique, which confirmed this assumption. Further scientific studies also reported the appearance of dynamic recrystallization at high temperatures above 300 °C for the precipitation-hardenable AA7075 alloy [18,19].

This process of dynamic recrystallization and the associated grain growth during hot forming affects not only the forming behavior, but also the microstructural evolution during the hot-forming of precipitation-hardenable aluminum alloys, which sets the desired mechanical properties after the thermo-mechanical treatment [20–22]. For this reason, knowledge of complex precipitation kinetics and precipitation–dislocation interactions in high-strength aluminum alloys, such as AA7075, is necessary to obtain a better understanding of the microstructure and mechanical properties after processing [23–25]. Plastic deformation during an integrated forming process has the ability to control the size and distribution of precipitates [26]. The plastic deformation is accompanied by a high dislocation density and crystal lattice defects inside the material, which can induce changes in the precipitation sequence and can affect the final material strength after the aging treatment [27,28]. Jung et al. investigated the effect of plastic deformation at different temperatures on the aging behavior of AA7075 [29]. The experimental results in this study showed an increase in the mechanical properties of the material formed at elevated temperatures with the increase in the deformation level. The related microstructure of the formed material represents a homogeneous distribution of fine precipitates after aging treatment, leading to a high material strength.

Therefore, taking the above-described observations into account, microstructural changes induced by the new thermo-mechanical process approach may be of great importance as the precipitation morphology and their distribution can lead to fundamental changes in the material properties. Moreover, different levels of pre-strains at elevated temperatures, as shown in the literature, can lead to dissimilar mechanical properties and, consequently, inhomogeneous hardness distributions of the formed part. Concerning the described hot stamping process for high-strength aluminum alloys, where the forming process is integrated immediately after solutionizing using forming tools with different contours and radii, an inhomogeneous material strength can be obtained as a result of hot deformation. However, only a few research works exist in this regard with a focus on the influences of plastic deformation at elevated temperatures on the resulting material hardness and local strength. For this reason, the aim of this work was to investigate the impact of deformation degree at high temperatures on the microstructure and the mechanical properties of precipitation-hardenable AA7075.

## 2. Materials and Methods

### 2.1. Materials and Testing Procedures

The experimental investigation in this study was carried out on precipitation-hardenable aluminum alloy AA7075 (Al-Zn-Mg (-Cu)), which is used commonly in the aerospace industry [23]. The chemical composition of the material is given in Table 1. The as-received material condition, supplied by AMAG (Austria Metal AG), was T6 (solution-heat-treated, quenched, and artificially aged) with a hardness level of 189 HV5 and an ultimate tensile strength of 577 MPa at room temperature. Depending on the selected thermo-mechanical process, the investigated materials were sectioned into blanks of 250 × 140 × 1.5 mm.

Specimens for hot deformation tensile tests were machined by electrical discharge machining with a gauge length and width of 45 and 7.5 mm, respectively. All tensile specimens were taken along the rolling direction. The cross-sectional speed during deformation at elevated temperature was set to 10 mm/min. Strengthening effects were reflected

after aging treatment using Vickers hardness measurements (EMCO DuraScan, Salzburg, Austria) to visualize the material hardness distribution.

**Table 1.** Chemical composition of the investigated alloy AA7075 determined by optical emission spectroscopy, according to AMAG (Austria Metal AG).

Chemical Elements (wt.%)	Si	Fe	Cu	Mn	Mg	Cr	Zn	Ti	Others
AA7075—as received (AR)	0.08	0.12	1.6	0.04	2.7	0.19	5.9	0.05	0.03

In order to identify the related geometrical changes and the deformation zone, the digital image correlation (DIC) technique was performed at elevated temperatures. For this aim, a contrast surface pattern was created using two different colors sprayed to apply a speckle pattern. For image acquisition, a CCD camera (Schneider Kreuznach—Xenoplan, Bad Kreuznach, Germany 2.8/50-0511 with a resolution of  $1280 \times 1024$  pixels) was focused on the measured sample zone, recording at a rate of 6 Hz. The strain calculation was performed using the obtained image by the ARAMIS v6.1 software (GOM—Gesellschaft für Optische Messtechnik mbH, Braunschweig, Germany). For the strain calculation, a facet size of  $12 \times 11$  was selected for all measurements.

Microstructure investigations were conducted using a transmission electron microscope JEOL JEM 2100 HRTEM, Tokyo, Japan operated at 200 kV. Discs of 3 mm were first grinded to  $\sim 150 \mu\text{m}$  and then electro-polished with an electrolyte solution of 25% nitric acid + 75% methanol. Imaging of the microstructural changes was carried out using a CCD camera (Model 833 Orius SC200D, Gatan, Pleasanton, CA, USA). Moreover, the as-received microstructure was investigated using a field emission scanning electron microscope (SEM, Carl Zeiss Microscopy GmbH, Köln, Germany) by the backscattered electron (BSE) contrast technique operating at a nominal voltage of 20 kV to visualize the precipitates' morphology before the thermo-mechanical process. For this aim, mechanical preparation by standard grinding and polishing (colloidal silica solution for final polishing) was carried out for microstructure examination.

## 2.2. Experimental Setup and Program

As this work focused on the above-mentioned novel forming process for the production of complex-shaped thin-walled high-strength aluminum parts, due to a large number of scientific and industrial studies indicating its feasibility and successful application in the automotive industry, the chosen hot forming parameters were derived from the results of those studies [8,28,30–32].

The main experimental setup in the present study consisted of a roller hearth furnace for solutionizing the sheet material and a hydraulic press (MAE DE Erkrath, Germany, 400 Z 160) with a press capacity of 4000 kN equipped with hat-shaped forming tools. For the artificial aging treatment, a chamber furnace (ThermConcept, Bremen, Germany, KM 710/13) was used to achieve a homogeneous temperature distribution (Figure 1a) [33,34].

Moreover, to emulate the selected thermo-mechanical process and to precisely investigate the influence of defined deformation degrees on the material hardness and microstructural changes, a tensile testing machine (Hegewald- und Peschke Inspekt Table Blue, Nossen, Germany) equipped with a moveable inductor and contact cooling devices was used (Figure 1b). This setup allows controlled heating, straining to defined plastic deformation levels, and the cooling of the fixed sample within the testing machine. The heating rate was set to  $20 \text{ }^\circ\text{C/s}$  at a frequency of 224 kHz. Immediately after completion of the heating, solutionizing, and forming operations at the elevated temperature, cooling of the fixed samples was carried out using cooling devices (Figure 1b). With these devices, a cooling rate of  $190 \text{ }^\circ\text{C/s}$  between  $400 \text{ }^\circ\text{C}$  and  $200 \text{ }^\circ\text{C}$  was achieved, measured with thermocouples fixed on the tensile sample. Preliminary tests proved that this cooling rate was sufficient to achieve mechanical properties comparable to those under the T6-condition.

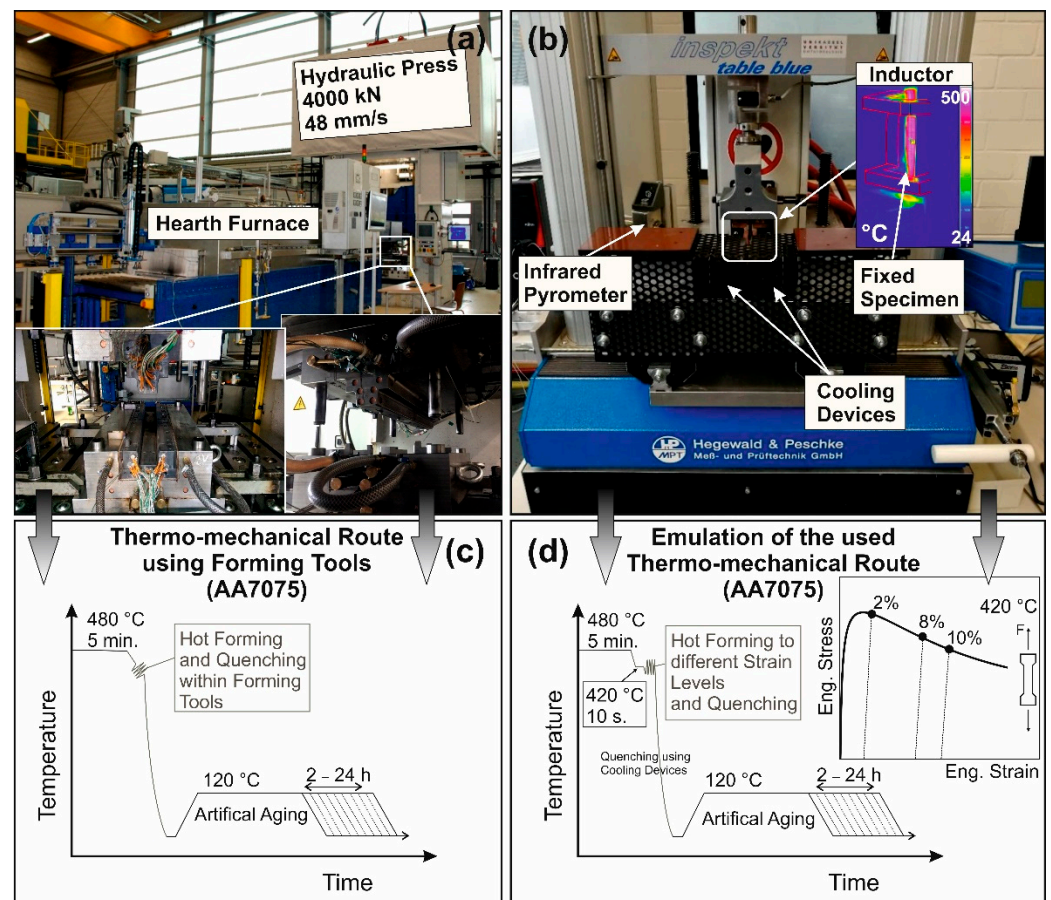


**Figure 1.** Selected experimental setups: (a) roller hearth furnace and press with forming tool, (b) tensile machine equipped with heating and cooling devices to emulate the thermo-mechanical process, and (c,d) schematic illustration of process routes and corresponding process parameters. Adapted from [31]. In (c), the process parameters of the thermo-mechanical forming and subsequent aging are shown. After solution treatment, the sheet material is hot-formed and quenched within the forming tools. In (d), the selected parameters for the emulated forming process are illustrated. The heated material is cooled to the forming temperature of 420 °C after solution treatment and is then held for 10 s to obtain a homogenous temperature to emulate the heat losses during the sheet transfer and tool closure. Immediately after completion of the controlled hot deformation ranging from 2 to 10% at 420 °C, the specimen is quenched using cooling devices.

The first set of experiments in this study focused on the effect of hot deformation on the material hardness under the as-quenched condition immediately after tool cooling. For this aim, the investigated sheet material was heated to the recommended solution heat treatment temperature of 480 °C and was soaked for 5 min. After completion of the solutionizing, the heated blanks were formed and quenched within the cooled forming tools to create the supersaturated solid solution at room temperature (Table 2). Immediately after quenching, samples were taken from the formed part and tested using a Vickers hardness measurement machine to obtain the material hardness distribution.

In the second group of experiments, the process parameters from the first group were taken to emulate the forming process and to adjust the different defined deformation levels after solution heat treatment. For this aim, the temperature of the tensile specimen after solution heat treatment was reduced from 480 °C over 5 min to the forming temperature of 420 °C, and it was held for 10 s to obtain a homogenous temperature distribution. After 10 s, the investigated material was formed to 2, 8, and 10%, and it was quenched within the cooling devices to create, similar to the first group of experiments, a supersaturated solid solution (Table 2). Analogous to the first group, samples were tested immediately



after cooling using the hardness measurement to clarify the effect of different deformations of the material hardness under the as-quenched condition.

**Table 2.** Experimental parameters for the investigation of the forming process. TM: thermo-mechanical process. ETM: emulated thermo-mechanical process.

Material	SHT Temperature (°C)	SHT Time (s)	Forming Temperature (°C)	Cooling	Aging
AA7075 (TM)	480	300	~420	Forming tool	-
AA7075 (ETM)	480	300	420	Cooling device	-
AA7075 (TM)	480	300	~420	Forming tool	120 °C—(2, 20, 24) h
AA7075 (ETM)	480	300	420	Cooling device	120 °C—(2, 6, 12, 16, 20, 24) h

The third group of experiments (TM), Figure 1c, aimed to investigate the novel thermo-mechanical forming process on the hardness distribution of the formed parts after different aging parameters. For this purpose, the investigated material was first heated to the in-literature recommended solution heat treatment temperature of 480 °C and was then soaked for 5 min [35]. After the manual transfer in around 6–8 s, the heated material was formed and quenched within the cooled tools, Table 2. The temperature of the tools was set to 24 °C using an internal water cooling system. The aging treatment was then carried out at a temperature of 120 °C from 2 to 24 h.

In the last group of experiments (ETM), the same process parameters as in the first group were selected to emulate the thermo-mechanical process and to investigate the effect of the defined deformation level on the material hardness, as well as on precipitation kinetics (Figure 1d). For this aim, inductive heating was employed to heat the specimen to 480 °C. After the solution heat treatment for 5 min, the sample temperature was reduced to the forming temperature of 420 °C and then held for 10 s to obtain a homogeneous temperature distribution. Immediately after the completion of the deformation (2, 8, and 10%), the sample was quenched using the cooling devices. Before mechanical testing, the samples were artificially aged at 120 °C for 2 to 24 h.

### 3. Results

#### 3.1. Forming Behavior at Elevated Temperature

The forming, as well as the local deformation, behavior at 420 °C after solutionizing the investigated material AA7075 is shown in Figure 2. The ultimate tensile strength of 18 MPa was obtained at a very low strain level (Figure 2a). After reaching the peak stress, the tensile curve decreased steadily and an increased true strain to failure was observed compared to those at room temperature reported in the literature for AA7075 [36]. In the present case, a maximum true strain of 0.315 was achieved.

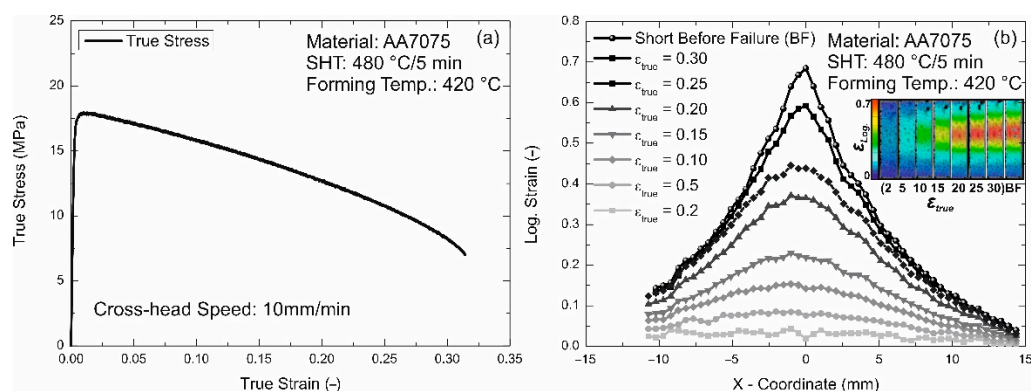


**Figure 2.** (a) Hot forming behavior of AA7075 at 420 °C after solution heat treatment and the corresponding (b) evolution of local deformation along the sample surface up to short before failure (BF).

The local deformation behavior along the tensile axis of the heated specimen obtained by the DIC-system is displayed in Figure 2b. The strain distribution was taken simultaneously during the tensile deformation at a forming temperature of 420 °C and a cross-head speed of 10 mm/min. In this figure, an almost homogeneous local deformation appeared at a very early stage of deformation (up to a true strain level of 0.10). With the further increase in plastic deformation, a high local deformation arose in the middle of the tensile specimen. This behavior was observed in the strain map received by DIC measurements, Figure 2b. The magnitude of the obtained local deformation from the strain map rose to a very high value of  $\epsilon_{\text{Log}} = 0.7$ , which is an indicator for the high ductility of this material at elevated temperatures also observed in the tensile curve in Figure 2a.

### 3.2. As-Received Microstructure and Mechanical Properties

The as-received microstructure of the investigated AA7075 alloy is given in Figure 3a using the backscattered electron contrast. It shows a finely distributed particle morphology within the studied grain structures. Such fine and dispersed precipitates are known to significantly enhance the strength of the precipitation-hardenable aluminum alloys due to their interaction with dislocations also reflected by the resulting stress–strain behavior of the as-received condition in Figure 3b. In addition to these particles in the grain interior, relatively coarse precipitates appeared along the grain boundaries [37]. The occurrence of these relatively coarse precipitates could also be observed in the grain interiors. Coarse-sized and irregularly distributed precipitates in the AA7075 alloy are usually referred to as  $\eta$ -phases, which can remain after the hot rolling process [38]. In Figure 3b, the stress–strain behavior of the hot formed material after artificial aging is given in comparison to the as-received condition. From this figure, a slight increase in yield and ultimate tensile strength for the hot formed material could be seen. Both curves indicate high material strengths, which can be explained by the formation of the strengthening  $\eta'$ -phases, as observed in Figure 3a for AA7075 [36].

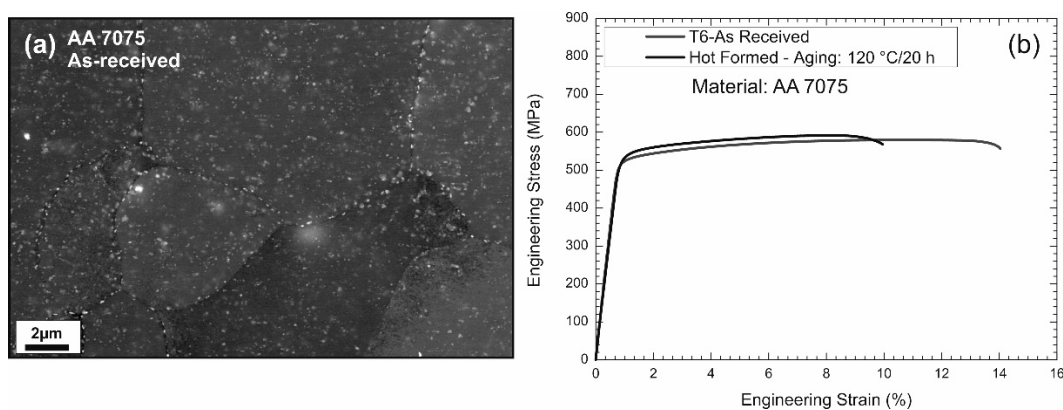


**Figure 3.** (a) Backscattered electron (BSE) micrographs of the investigated material under the T6 as-received condition before thermo-mechanical processing. (b) Stress–strain behavior of the formed parts using the novel forming process compared to the as-received condition.

### 3.3. Effect of Hot Deformation under As-Quench Condition

The mechanical properties of the investigated alloy immediately after the forming operation and quenching is shown in Figure 4a,b. For the formed hat-profile, a homogenous hardness distribution was observed along the measured zone (Figure 4a). The highest obtained hardness level for the formed part under the as-quenched condition was 107 HV5. In the zones with a high deformation degree (radii R1 and R2), no significant difference or an increase in material hardness was observed. The resulting material hardness for the emulated forming process revealed, for all deformation levels, almost the same material hardness (Figure 4b). Interestingly, with increase in the deformation level, the hardness

level of the material remained almost unchanged. Even after hot forming to a high strain level of 10%, no remarkable rise in material hardness could be found.

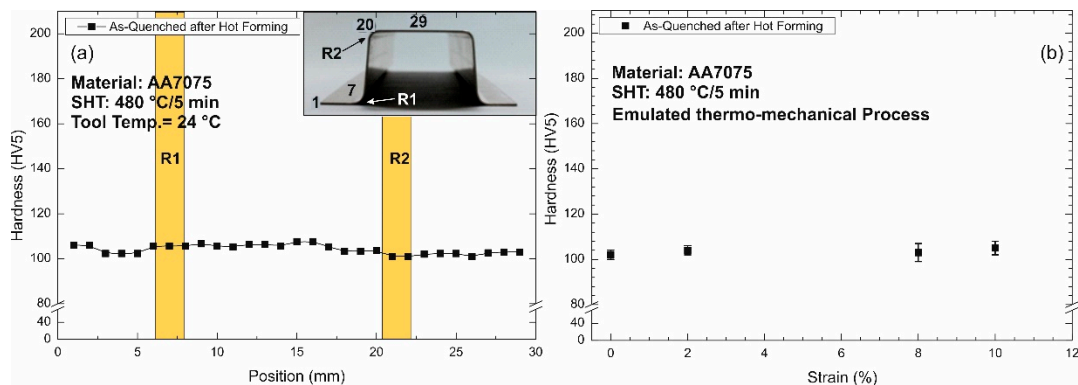


**Figure 4.** (a) The as-quenched hardness distribution of the formed hat-profile after the hot forming and cooling within the novel forming process, and (b) the resulting material hardness after different deformation levels within the emulated thermo-mechanical process (radii of the formed part: R1 and R2).

### 3.4. Effect of Hot Deformation on the Strengthening Behavior after Artificial Aging

The property distribution of hot-formed parts under industrial process conditions was investigated in the present study on examples of a hat profile (Figure 5a) after hot forming and different aging processes, cf. Figure 1c. The lowest hardness distribution was obtained for the material aged at 120 °C for 2 h (Figure 5a). With increasing aging time up to 24 h, the hardness values increased. Under all conditions, fluctuations in the hardness level appeared along the measured zone. This behavior was more pronounced for the material aged at 20 and 24 h. Interestingly, in Figure 5a, the zones with significantly higher deformation degrees (radii R1 and R2) showed, compared to the top side of the hot-formed geometry, no noticeable rise in the hardness level. However, a significant decrease in the obtained hardness in the center of the top-hat section was noticed for all conditions, probably a result of the local cooling conditions.

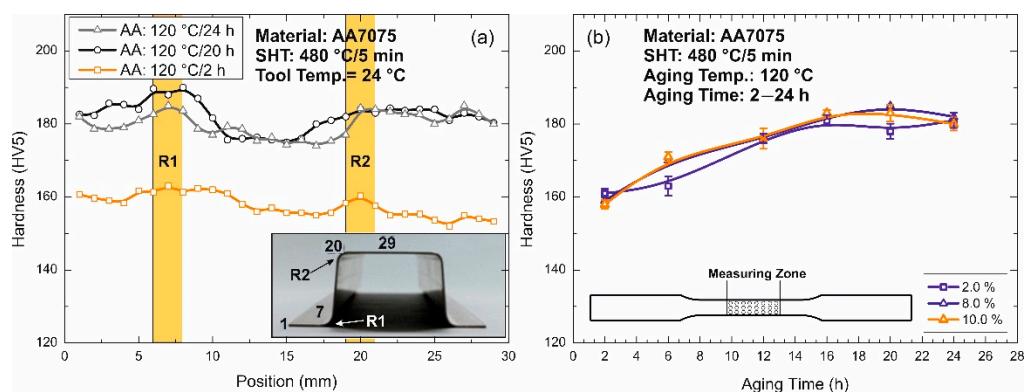


**Figure 5.** (a) Hardness profile of the hot-formed components after different artificial aging (AA) times. The sheet materials were first solution-annealed and then quenched within the forming tools. (b) Hardness evolution of samples at different deformation levels and aging times of emulated process route. The zone of 15 mm × 7.5 used for hardness measurement for all formed conditions is shown in (b).

The hardness distribution after emulation of the thermo-mechanical process route at different deformation degrees of 2, 8, and 10% and different artificial aging (AA) times ranging from 2 to 24 h is shown in Figure 5b. For all forming conditions, a hardness level of almost 160 HV5 was found after 2 h of artificial aging. With the increase in the aging time to 20 h, the material hardness values of the hot-formed material at 8 and 10% of deformation

increased to a maximum level of 185 HV5. For the same aging temperature and time, the 2%-hot-formed material showed a hardness value of 179 HV5 accordingly. A further increase in the aging time to 24 h resulted in minor decreases in the material hardness of the hot-formed material at 8 and 10%. Both conditions revealed almost identical hardness evolutions after attaining the peak stress. In contrast, the hardness level of the hot-formed material at 2% increased slightly after aging at 120 °C for 24 h. However, by comparing the hardness evolution of all conditions, the deformation level seemed to have no noticeable influence on the hardness level.

### 3.5. Effect of Hot Deformation on Microstructure

TEM investigations were conducted after artificial aging to investigate the influence of the hot deformation on the resulting precipitation morphology, probably explaining the effect on the material hardness, Figure 6. The microstructure of the at-2% hot-formed material showed, after aging at 120 °C for 20 h, a homogeneous distribution of very fine particles within the grain structure (Figure 6a,b). Under the same aging condition of AA7075, these very fine precipitations have been referred elsewhere in the literature to the  $\eta'$ -phase [36]. In addition, coarse precipitates were also observed in the center of the grains (Figure 6a), which were also reported in literature [35,36] for the same aging treatment of AA7075. In Figure 6b, few dislocations were presented in the investigated microstructure. Interestingly, near to dislocations, there were zones with a high density of coarse particles and other zones with a lower number of precipitates. However, dislocation–precipitation interaction was not directly observed.

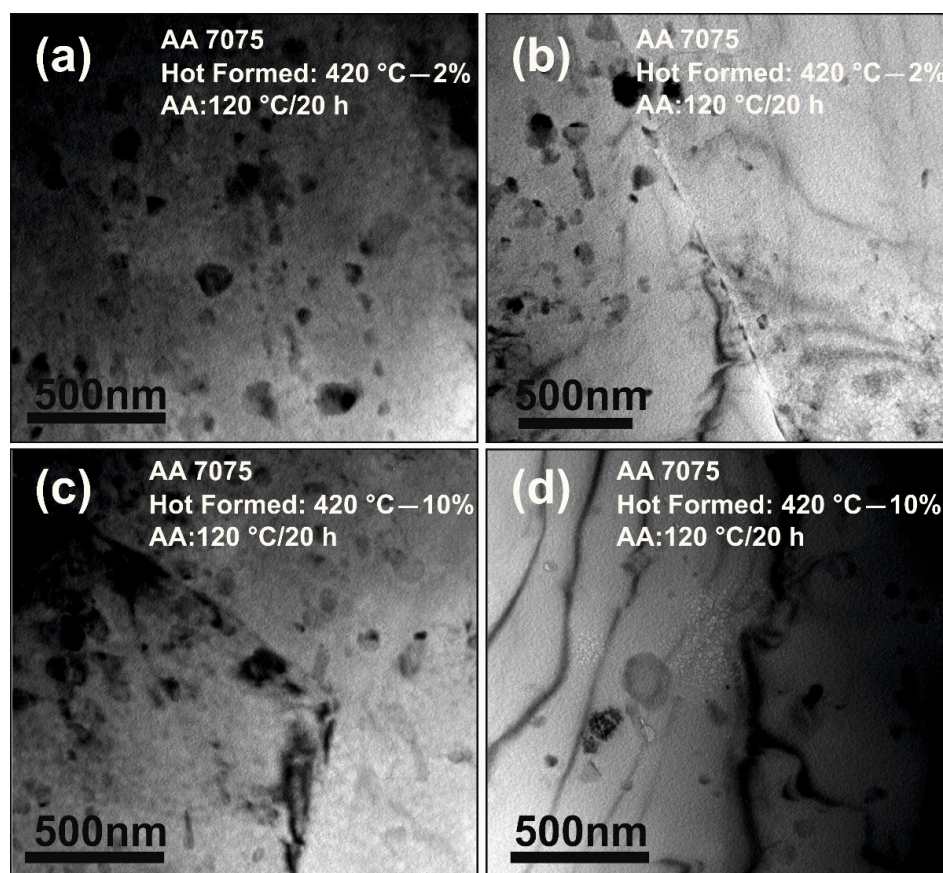


**Figure 6.** TEM micrographs of the at 420 °C-formed materials of (a,b) 2% and (c,d) 10% of deformation. All samples were solution-heat-treated at 480 °C for 5 min and were artificially aged at 120 °C for 20 h.



Figure 6c,d display the microstructure after aging at 120 °C for 20 h of the material hot-formed at 10%. Compared to the at 2% formed material, almost the same precipitation distribution and sizes were observed. Very small particles and some coarse particles were found in the grain structure (Figure 6c), as well as at grain boundaries. The diameter of these particles sometimes exceeded 100 nm. These particles are referred to as the stable  $\eta$ -phase [37,39]. Similar to at 2%, the at 10% hot-formed material also showed few dislocations.

#### 4. Discussion

The hot deformation behavior of the investigated material at 420 °C is shown in Figure 2. At the elevated temperature, an increased elongation to failure was observed for AA7075, indicating a better formability. The underlying reason may be attributed to the thermally activated softening mechanisms [40]. During the hot deformation, the occurrence of dynamic recovery and dynamic recrystallization leads to the formation of new grains and the reduction in dislocations, as well as in other defects inside the material [41]. Hence, these triggered phenomena cause significant changes in the deformed microstructure. The formation of new grains takes place by the consumption of dislocations and the reduction in the stored energy, leading to a decrease in the introduced deformation hardening associated with dislocations [42]. In addition, the heating of precipitation-hardenable aluminum alloys at temperatures slightly below the eutectic temperature dissolves precipitates, facilitating the dislocation movement [43]. Furthermore, the high thermal energy promotes dislocation gliding and dislocation climb [44].

The presented results of the hardness profile after hot forming and artificial aging revealed an increased material hardness after increasing the aging time, for both hat profiles and the ETM samples. This behavior is linked to the nucleation and growth of metastable GP-zones and the metastable hexagonal  $\eta'$ -phases. In this way, a high number of GP(II)-zones could exist in the microstructure at the beginning of the aging time, which would lead to a weak lattice distortion compared to coarser particles. The resulting misfit between the formed GP-zones and the aluminum matrix determines the geometry of the GP-zones [39]. With the increase in aging time, the size of the particles increases and a homogeneous structure is obtained after 20 h. Moreover, GP(II)-zones form into  $\eta'$ -phases and their shape changes [45]. At the optimum dimension of these nanosized particles, they constitute effective obstacles for dislocation movement, leading to a high material strength. In contrast, at a very short aging time of 2 h for AA7075, the size of the nucleated clusters and precipitates, as well as of the resulting interparticle spacing, is smaller, compared to the microstructure aged after 20 h. However, if the number of the nano-sized particles is higher for the 2 h aged condition, their size would be, on the other hand, much smaller, causing a less pronounced distortion of the surrounding matrix. As a result, resistance against dislocation motion decreases and relieves gliding processes during plastic deformation [44,46,47].

The slight decrease in hardness after 20 h of artificial aging at 120 °C for the material hot-formed at 8 and 10% can be linked to an increased number of  $\eta$ -precipitates ( $\text{MgZn}_2$ ), as well as a growth of  $\eta'$ -phases. This phenomenon is triggered by the transformation of GP-zones into stable phases and the promoted high diffusion rate of the solutes due to the elevated aging temperature. Several imperfections in the crystal lattice structure, e.g., high concentration of vacancies, as well as a high dislocation density, can activate the formation of precipitates. Both can act as a nucleation source and sink, enhancing the precipitation nucleation rate by an extensively high diffusion rate of solutes within the grain interior [23,29,48,49]. However, by comparing all emulated conditions, the obtained material hardness of the hot-formed microstructures after an artificial aging at 120 °C for 20 h indicated no dramatic or significant differences. This behavior may be a result of the softening mechanisms, activated by the plastic deformation at the hot forming temperature, leading to a decrease in dislocation density. Despite this, a slight decrease was obtained when exceeding 20 h of aging for the samples hot-formed at 8 and 10%. The underlying

mechanisms during hot forming and their influence on material hardness is addressed in detail in the following section.

The detailed analysis of the localized plastic deformation distribution of the hat profiles points to an inhomogeneous hardness distribution along the measured zone. This inhomogeneity was more pronounced at higher aging times. A clear decrease in hardness could be seen in the side wall of the formed profile, Figure 5a, which was presumably due to the cooling conditions of the sheet material during hot forming operation. Interestingly enough, no noticeable rise in material hardness in the locally highly deformed zones, the radii of the hat profile, was obtained. The detailed investigation of this phenomenon by an emulation of the thermo-mechanical process on a tensile testing machine (Figure 1b) revealed that, with the increase in the hot deformation level from 2% to 10% at 420 °C, the SMT-specimens exhibited no significant increase in material hardness. A possible explanation may be the activation of softening mechanisms during hot deformation. At low forming temperatures, when no recrystallization occurs, plastic deformation can lead to a dramatic increase in dislocation density [50]. At higher temperatures, in contrast, plastic deformation promotes the activation of softening mechanisms, such as dynamic recrystallization, which ultimately reduce the dislocation density by consuming dislocations, and grain boundary migration by the coarsening of subgrains [51–53]. Therefore, a lower dislocation density than expected was obtained at 420 °C for the 10%-formed material, which did not promote the nucleation of precipitates or accelerate the precipitation kinetics. Nevertheless, the TEM micrographs revealed almost the same precipitation behavior for the hot-formed material independently of the deformation level. As the range of the chosen deformation level of 2–10% may not be sufficient, further microstructural investigations are needed to better-understand the precipitation behavior after hot deformation, which will be the focus of future studies.

Another interesting observation in this study was the change in the hardness distribution pattern after artificial aging. Initially, as can be seen in Figure 4a, the condition immediately after tool quenching revealed an almost homogeneous hardness distribution. Then, the artificial aging of the as-quenched microstructure led to a general increase in the hardness level, as well as to an inhomogeneous hardness distribution along the measured distance (Figure 5a). The inhomogeneous hardness pattern is linked to the particular cooling conditions within the hat-profile forming process, as the precipitation formation and, consequently, the mechanical properties of the investigated alloy was strongly affected by the cooling rate and the degree of supersaturation after quenching. Considering this fact, during the forming and quenching operation, the nonuniform contact conditions between the sheet and tool could lead to an inhomogeneous temperature distribution of the pre-heated sheet material, resulting in different local cooling rates and the creation of a microstructure with different solute atom concentrations. In this manner, zones with lower cooling rates would contain few coarse quench-induced precipitates and lower solute atom concentrations for nucleation and growth of strengthening particles during artificial aging. Under the as-quenched condition, the strength difference between zones of different levels of supersaturation was not very large, as the few already nucleated particles did not contribute significantly to the material strength. However, during artificial aging, zones with locally higher solute atom concentrations favored the extensive formation of strengthening precipitates, whereas zones with lower levels of supersaturation did not develop the same precipitation rate. This behavior may have led to the observed inhomogeneous material hardness after artificial aging.

## 5. Conclusions

The influence of deformation degree at elevated temperatures on the precipitation kinetics of AA7075 was investigated in this study with the following conclusions:

- The formation of a high-strength aluminum alloy at a high temperature of 420 °C led to a higher formability compared to room-temperature forming due to the activated softening mechanisms.

- The response of artificial aging to the hot deformation represented only a low influence on mechanical properties due to dynamic recrystallization and recovery, leading to a decrease in dislocation density.
- Almost the same microstructure with the nucleation of fine precipitates, which act as effective barriers to dislocation motion, as well as few coarse particles, were obtained at hot deformations of 2% and 10%, confirming the low effect of the deformation degree.
- Nonetheless, further microstructural investigations are needed to clarify the complex precipitation–dislocation behavior during artificial aging.

**Author Contributions:** Conceptualization, E.S. and U.W.; methodology, E.S., D.S. and S.B.; investigation, E.S., D.S. and S.B.; writing—original draft preparation, E.S. and U.W.; writing—review and editing, E.S., U.W. and K.S.; visualization, E.S.; supervision, U.W. and K.S. All authors have read and agreed to the published version of the manuscript.

**Funding:** The author would like to thank the Hessen State Ministry for Higher Education, Research and the Arts—Initiative for the Development of Scientific and Economic Excellence (LOEWE), for the financial support of the special research project “ALLEGRO”.

**Institutional Review Board Statement:** Not applicable.

**Informed Consent Statement:** Not applicable.

**Data Availability Statement:** Not applicable.

**Acknowledgments:** The authors would like to thank Dipl.-Ing. Stefan Seidel for sample preparation.

**Conflicts of Interest:** The authors declare no conflict of interest. The hot forming process is a registered trademark of Impression Technologies Limited.

## References

1. Starke, E.A.; Staley, J.T. Application of Modern Aluminum Alloys to Aircraft. *Prog. Aerosp. Sci.* **1996**, *32*, 131–172. [[CrossRef](#)]
2. Hornbogen, E.; Starke, E.A. Overview no. 102 Theory assisted design of high strength low alloy aluminum. *Acta Metall. Mater.* **1993**, *41*, 1–16. [[CrossRef](#)]
3. Peng, X.; Fan, J.; Yang, Y.; Chen, Y.; Yin, Y. Investigations to the effect of heating-rate on the mechanical properties of aluminum alloy LY12. *Int. J. Solids Struct.* **2003**, *40*, 7385–7397. [[CrossRef](#)]
4. Garrett, R.P.; Lin, J.; Dean, T.A. An investigation of the effects of solution heat treatment on mechanical properties for AA 6xxx alloys: Experimentation and modelling. *Int. J. Plast.* **2005**, *21*, 1640–1657. [[CrossRef](#)]
5. Krajewski, P. Overview of Quick Plastic Forming Technology. *Mater. Sci. Forum* **2007**, *551–552*, 3–12. [[CrossRef](#)]
6. Bay, N. Cold forming of aluminium—state of the art. *J. Mater. Process. Technol.* **2000**, *71*, 76–90. [[CrossRef](#)]
7. Lin, J.; Balint, D.S.; Wang, L.; Trevor, A.D.; Foster, A.D. Method of Forming A Component of Complex Shape from Sheet Material. U.S. Patent No. 9,950,355, 24 April 2018.
8. El Fakir, O.; Wang, L.; Balint, D.; Dear, J.P.; Lin, J.; Dean, T.A. Numerical study of the solution heat treatment, forming, and in-die quenching (HFQ) process on AA5754. *Int. J. Mach. Tools Manuf.* **2014**, *87*, 39–48. [[CrossRef](#)]
9. Scharifi, E.; Knoth, R.; Weidig, U. Thermo-mechanical forming procedure of high strength Aluminum sheet with improved mechanical properties and process efficiency. *Procedia Manuf.* **2019**, *29*, 481–489. [[CrossRef](#)]
10. Zheng, K.; Dong, Y.; Zheng, J.H.; Foster, A.; Lin, J.; Dong, H.; Dean, T.A. The effect of hot form quench (HFQ<sup>®</sup>) conditions on precipitation and mechanical properties of aluminium alloys. *Mater. Sci. Eng. A* **2019**, *761*, 138017. [[CrossRef](#)]
11. Zheng, K.; Politis, D.J.; Wang, L.; Lin, J. A review on forming techniques for manufacturing lightweight complex—Shaped aluminium panel components. *Int. J. Light. Mater. Manuf.* **2018**, *1*, 55–80. [[CrossRef](#)]
12. Sajadifar, S.V.; Moieni, G.; Scharifi, E.; Lauhoff, C.; Böhm, S.; Niendorf, T. On the Effect of Quenching on Postweld Heat Treatment of Friction-Stir-Welded Aluminum 7075 Alloy. *J. Mater. Eng. Perform.* **2019**, *28*. [[CrossRef](#)]
13. Liu, J.; Gao, H.; El Fakir, O.; Wang, L.; Lin, J. HFQ forming of AA6082 tailor welded blanks. *MATEC Web Conf.* **2015**, *21*, 05006. [[CrossRef](#)]
14. Li, N.; Mohamed, M.S.; Cai, J.; Lin, J.; Balint, D.; Dean, T.A. Experimental and numerical studies on the formability of materials in hot stamping and cold die quenching processes. *AIP Conf. Proc.* **2011**, *1353*, 1555–1561. [[CrossRef](#)]
15. Garrett, R.P.; Lin, J.; Dean, T.A. Solution Heat Treatment and Cold Die Quenching in Forming AA 6xxx Sheet Components: Feasibility Study. *Adv. Mater. Res.* **2005**, *6–8*, 673–680. [[CrossRef](#)]
16. Wang, L.; Strangwood, M.; Balint, D.; Lin, J.; Dean, T.A. Formability and failure mechanisms of AA2024 under hot forming conditions. *Mater. Sci. Eng. A* **2011**, *528*, 2648–2656. [[CrossRef](#)]

17. Sajadifar, S.V.; Scharifi, E.; Weidig, U.; Steinhoff, K.; Niendorf, T. Performance of Thermo-Mechanically Processed AA7075 Alloy at Elevated Temperatures—From Microstructure to Mechanical Properties. *Metals* **2020**, *10*, 884. [[CrossRef](#)]
18. Xiao, W.; Wang, B.; Wu, Y.; Yang, X. Constitutive modeling of flow behavior and microstructure evolution of AA7075 in hot tensile deformation. *Mater. Sci. Eng. A* **2018**, *712*, 704–713. [[CrossRef](#)]
19. Gupta, R.K.; Anil Kumar, V.; Sarath Krishnan, A.; Niteshraj, J. Hot Deformation Behavior of Aluminum Alloys AA7010 and AA7075. *J. Mater. Eng. Perform.* **2019**, *28*, 5021–5036. [[CrossRef](#)]
20. Shojaei, K.; Sajadifar, S.V.; Yapici, G.G. On the mechanical behavior of cold deformed aluminum 7075 alloy at elevated temperatures. *Mater. Sci. Eng. A* **2016**, *670*, 81–89. [[CrossRef](#)]
21. Lin, Y.C.; Chen, X.M. A critical review of experimental results and constitutive descriptions for metals and alloys in hot working. *Mater. Des.* **2011**, *32*, 1733–1759. [[CrossRef](#)]
22. Sakai, T.; Belyakov, A.; Kaibyshev, R.; Miura, H.; Jonas, J.J. Progress in Materials Science Dynamic and post-dynamic recrystallization under hot, cold and severe plastic deformation conditions. *Prog. Mater. Sci.* **2014**, *60*, 130–207. [[CrossRef](#)]
23. Hornbogen, E. Hundred years of precipitation hardening. *J. Light Met.* **2001**, *1*, 127–132. [[CrossRef](#)]
24. Jäggle, E.A.; Sheng, Z.; Wu, L.; Lu, L.; Risse, J.; Weisheit, A.; Raabe, D. Precipitation Reactions in Age-Hardenable Alloys during Laser Additive Manufacturing. *JOM* **2016**, *68*, 943–949. [[CrossRef](#)]
25. Lin, Y.C.; Jiang, Y.Q.; Chen, X.M.; Wen, D.X.; Zhou, H.M. Effect of creep-aging on precipitates of 7075 aluminum alloy. *Mater. Sci. Eng. A* **2013**, *588*, 347–356. [[CrossRef](#)]
26. Segal, V.M. New hot thermo-mechanical processing of heat treatable aluminum alloys. *J. Mater. Process. Technol.* **2016**, *231*, 50–57. [[CrossRef](#)]
27. Zheng, J.H.; Dong, Y.; Zheng, K.; Dong, H.; Lin, J.; Jiang, J.; Dean, T.A. Experimental investigation of novel fast-ageing treatments for AA6082 in supersaturated solid solution state. *J. Alloys Compd.* **2019**, *810*, 151934. [[CrossRef](#)]
28. Li, N.; Zheng, J.; Zhang, C.; Zheng, K.; Lin, J.; Dean, T.A. Investigation on fast and energy-efficient heat treatments of AA6082 in HFQ processes for automotive applications. *MATEC Web Conf.* **2015**, *21*, 05015. [[CrossRef](#)]
29. Jung, S.H.; Lee, J.; Kawasaki, M. Effects of pre-strain on the aging behavior of Al 7075 alloy for hot-stamping capability. *Metals* **2018**, *8*, 137. [[CrossRef](#)]
30. Vrolijk, M.; Koroschetz, C.; Holecek, M.; Snilsberg, K.E.; Jönsson, L.-O.; Anyasodor, G.; Lorenz, D. Investigation on Aluminium Hot and Warm Forming with the Help of Virtual Process Modeling. In Proceedings of the 6th International Seminar on Hot Sheet Metal Forming of High-Performance Steel CHS2, Atlanta, GA, USA, 4–7 June 2017; pp. 673–681.
31. Scharifi, E.; Schade, T.; Ademaj, A.; Sajadifar, S.V.; Weidig, U.; Niendorf, T.; Steinhoff, K. Characterization of Mechanical Properties, Macroscopic Deformation Behavior, and Microstructure of Functionally Graded 22MnB5 Steel. *Steel Res. Int.* **2000**, 633. [[CrossRef](#)]
32. Mohamed, M.S.; Foster, A.D.; Lin, J.; Balint, D.S.; Dean, T.A. Investigation of deformation and failure features in hot stamping of AA6082: Experimentation and modelling. *Int. J. Mach. Tools Manuf.* **2012**, *53*, 27–38. [[CrossRef](#)]
33. Scharifi, E.; Sajadifar, S.V.; Moeini, G.; Weidig, U.; Böhm, S.; Niendorf, T.; Steinhoff, K. Dynamic Tensile Deformation of High Strength Aluminum Alloys Processed Following Novel Thermomechanical Treatment Strategies. *Adv. Eng. Mater.* **2020**, *22*, 2000193. [[CrossRef](#)]
34. Heider, B.; Scharifi, E.; Engler, T.; Oechsner, M.; Steinhoff, K. Influence of heated forming tools on corrosion behavior of high strength aluminum alloys. *Mater. Werkst.* **2021**, *52*, 145–151. [[CrossRef](#)]
35. Sajadifar, S.V.; Scharifi, E.; Weidig, U.; Steinhoff, K.; Niendorf, T. Effect of Tool Temperature on Mechanical Properties and Microstructure of Thermo-Mechanically Processed AA6082 and AA7075 Aluminum Alloys. *HTM J. Heat Treat. Mater.* **2020**, *75*, 177–191. [[CrossRef](#)]
36. Scharifi, E.; Savaci, U.; Kavaklioglu, Z.B.; Weidig, U.; Turan, S.; Steinhoff, K. Effect of thermo-mechanical processing on quench-induced precipitates morphology and mechanical properties in high strength AA7075 aluminum alloy. *Mater. Charact.* **2021**, *174*, 111026. [[CrossRef](#)]
37. Zhao, H.; De Geuser, F.; Kwiatkowski da Silva, A.; Szczepaniak, A.; Gault, B.; Ponge, D.; Raabe, D. Segregation assisted grain boundary precipitation in a model Al-Zn-Mg-Cu alloy. *Acta Mater.* **2018**, *156*, 318–329. [[CrossRef](#)]
38. Marlaud, T.; Deschamps, A.; Bley, F.; Lefebvre, W.; Baroux, B. Influence of alloy composition and heat treatment on precipitate composition in Al-Zn-Mg-Cu alloys. *Acta Mater.* **2010**, *58*, 248–260. [[CrossRef](#)]
39. Buha, J.; Lumley, R.N.; Crosky, A.G. Secondary ageing in an aluminium alloy 7050. *Mater. Sci. Eng. A* **2008**, *492*, 1–10. [[CrossRef](#)]
40. Gao, H.; Weng, T.; Liu, J.; Li, C.; Li, Z.; Wang, L. Hot stamping of an Al-Li alloy: A feasibility study. *MATEC Web Conf.* **2015**, *21*, 05007. [[CrossRef](#)]
41. Maikranz-Valentin, M.; Weidig, U.; Schoof, U.; Becker, H.; Steinhoff, K. Components with Optimised Properties due to Advanced Thermo-mechanical Process Strategies in Hot Sheet Metal Forming. *Steel Res. Int.* **2008**, *79*, 92–97. [[CrossRef](#)]
42. Humphreys, F.J. Nucleation in recrystallization. *Mater. Sci. Forum* **2004**, *467–470*, 107–116. [[CrossRef](#)]
43. Fribourg, G.; Bréchet, Y.; Deschamps, A.; Simar, A. Microstructure-based modelling of isotropic and kinematic strain hardening in a precipitation-hardened aluminium alloy. *Acta Mater.* **2011**, *59*, 3621–3635. [[CrossRef](#)]
44. Zhou, M.; Lin, Y.C.; Deng, J.; Jiang, Y.Q. Hot tensile deformation behaviors and constitutive model of an Al-Zn-Mg-Cu alloy. *Mater. Des.* **2014**, *59*, 141–150. [[CrossRef](#)]
45. Edwards, G.A.; Stiller, K.; Dunlop, G.L.; Couper, M.J. The Precipitation Sequence in Al ± Mg ± Si Alloys. *Acta Mater.* **1998**, *46*, 3893–3904. [[CrossRef](#)]



46. Kumar, M.; Sotirov, N.; Chimani, C.M. Investigations on warm forming of AW-7020-T6 alloy sheet. *J. Mater. Process. Technol.* **2014**, *214*, 1769–1776. [[CrossRef](#)]
47. Lervik, A.; Marioara, C.D.; Kadanik, M.; Walmsley, J.C.; Milkereit, B.; Holmestad, R. Precipitation in an extruded AA7003 aluminium alloy: Observations of 6xxx-type hardening phases. *Mater. Des.* **2020**, *186*, 108204. [[CrossRef](#)]
48. Picu, R.C.; Zhang, D. Atomistic study of pipe diffusion in Al-Mg alloys. *Acta Mater.* **2004**, *52*, 161–171. [[CrossRef](#)]
49. Yang, B.; Milkereit, B.; Zhang, Y.; Rometsch, P.A.; Kessler, O.; Schick, C. Continuous cooling precipitation diagram of aluminium alloy AA7150 based on a new fast scanning calorimetry and interrupted quenching method. *Mater. Charact.* **2016**, *120*, 30–37. [[CrossRef](#)]
50. Jiang, H.; Sandlöbes, S.; Gottstein, G.; Korte-Kerzel, S. On the effect of precipitates on the cyclic deformation behavior of an Al-Mg-Si alloy. *J. Mater. Res.* **2017**, *32*, 4398–4410. [[CrossRef](#)]
51. McQueen, H.J.; Imbert, C.A.C. Dynamic recrystallization: Plasticity enhancing structural development. *J. Alloys Compd.* **2004**, *378*, 35–43. [[CrossRef](#)]
52. McQueen, H.J.; Ryan, N.D. Constitutive analysis in hot working. *Mater. Sci. Eng. A* **2002**, *322*, 43–63. [[CrossRef](#)]
53. Lv, J.; Zheng, J.-H.; Yardley, V.A.; Shi, Z.; Lin, J. A Review of Microstructural Evolution and Modelling of Aluminium Alloys under Hot Forming Conditions. *Metals* **2020**, *10*, 1516. [[CrossRef](#)]